

Modulation transfer function for infrared reflectarrays

Jose Antonio Gómez-Pedrero,^{1,*} James Ginn,² Javier Alda,¹ and Glenn Boreman^{2,3}

¹Applied Optics Complutense Group, University Complutense of Madrid, School of Optics, Avenue Arcos de Jalón, 118, 28037 Madrid, Spain

²Plasmonics Inc., 12565 Research Parkway, Suite 300, Orlando, Florida 32826, USA

³Department of Physics and Optical Science, University of North Carolina at Charlotte, Charlotte, North Carolina 28223, USA

*Corresponding author: jagomez@fis.ucm.es

Received 14 June 2011; revised 27 July 2011; accepted 27 July 2011;
posted 1 August 2011 (Doc. ID 149264); published 19 September 2011

The quality of the image produced by optical reflectarrays as a function of the $F/\#$, polarization, and wavelength is analyzed in this paper. The results are expressed as monochromatic and polychromatic modulation transfer functions. They show that large aperture multilevel reflectarrays perform quite close to the diffraction-limited case. The chromatic aberrations make these elements highly wavelength-selective. © 2011 Optical Society of America

OCIS codes: 160.3918, 050.5080, 110.3080.

1. Introduction

The use of electromagnetic resonant structures to modify the phase distribution of an incoming wavefront is opening the way for so-called resonant optics devices, which provide new design strategies for performance improvement of optical elements [1–3]. The basic units of resonant optics are subwavelength metallic structures above a reflective ground plane, placed according to regular or nonregular geometries, which interact electromagnetically with the incident electric field. The reradiated field is able to modify the spectral component, the polarization state, and the phase map of the resulting reflected wavefront [4–6]. Reflectarrays have been primarily used within the radio and microwave regime. In those bands, they perform extraordinarily well to conform and shape beam distributions in conjunction with classical antenna feed structures [7–9]. At higher frequencies close to the optical range, the material properties of metals constrain some of the design flexibility used at lower frequencies [10]. The strong attenuation of the currents generated

in the structures precludes the use of transmission line structures to extend the phase shift range, as is typically done in the microwave spectrum.

Recently, some designs of reflectarrays have been successfully fabricated and tested for use in the infrared band at $10.6\ \mu\text{m}$ [1,2]. They consist of a Fresnel zone arrangement that is selectively populated by resonant structures properly arranged in both shape and location to produce the desired phase shift on reflection. Then, the polarization, angular, and chromatic dependence of the resonances are superimposed, accounting for contributions coming from the Fresnel layout. The evaluation of the phase shift produced by the resonant structures is made using computational electromagnetics.

The modeling of the angular and polarization response has been made using two different computational tools: a finite-element package (HFSS by Ansoft) and a method-of-moments algorithm (Designer by Ansoft). The results of HFSS have been used previously to quantify the Strehl ratio for a reflectarray as a function of the aperture [3]. The complex reflection coefficient of the resonant element is expressed in Fig. 1 as a function of the angle, polarization state, and wavelength. The elements analyzed here correspond with a fabricated multilevel reflectarray

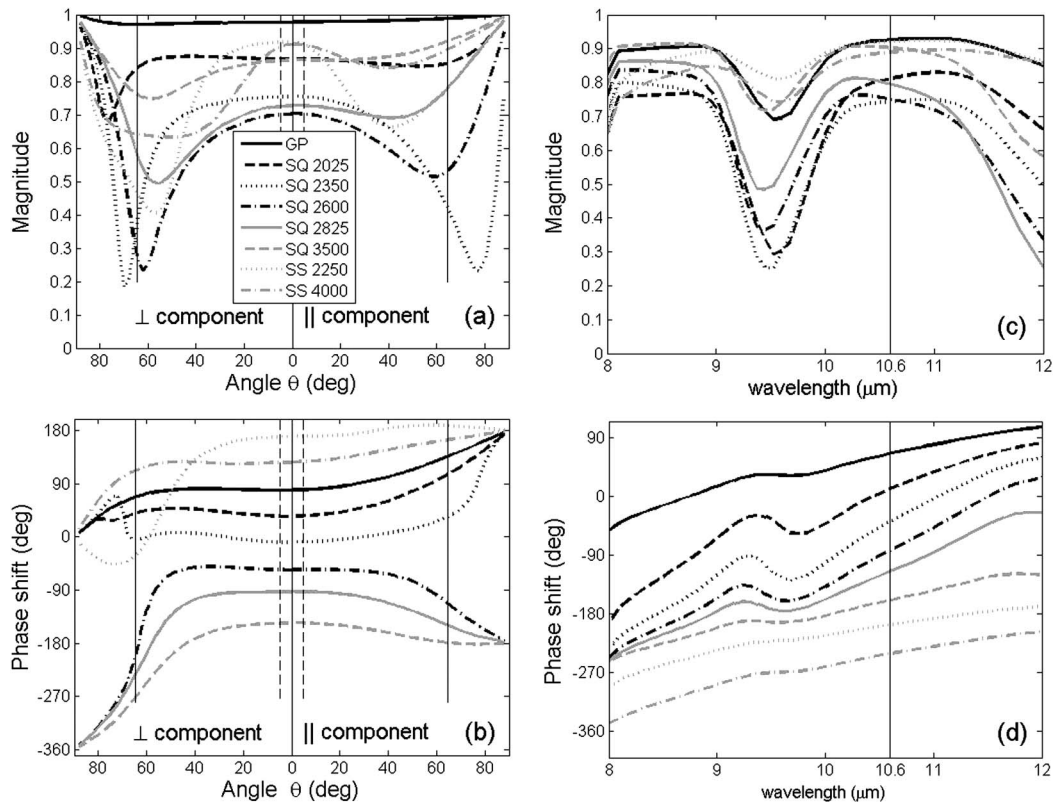


Fig. 1. Complex reflection coefficient for the eight different resonant structures used in this study. (a) and (c) represent the magnitude of the reflection coefficient. (b) and (d) represent the phase. The dependence with the angle for both polarization states is given in (a) and (b), meanwhile, the spectral behavior is presented in (c) and (d). The SQ labels are for square patches being the number of the value of the side of the square in nanometers. The SS labels are for square patch elements with slots introduced into the center of the element being the number of the size of the square slot in nanometers. GP denotes the ground plane. It is worth noticing that (a) and (b) have been computed using a finite-element method (HFSS by Ansoft) while (c) and (d) have been determined through a method-of-moments algorithm (Designer by Ansoft), which may explain the slight differences found for normal incidence and $10.6\text{ }\mu\text{m}$ wavelength.

working as a focusing mirror. The reflectarray is first designed using a Fresnel layout that sizes the radii of the Fresnel subzones in an eight-level arrangement. Nominally, the phase shift between adjacent Fresnel subzones is $\pi/4$. The Fresnel subzones are populated with resonant elements defined on a unit cell having a constant size along the reflectarray. In our case, the unit cell is a $5\text{ }\mu\text{m} \times 5\text{ }\mu\text{m}$ square and the resonant elements consist in a structure formed by a standoff layer grown on a metallic ground plane with a metallic patch deposited on top of the standoff layer. The form and size of this metallic patch determines the phase shift given by the region of the reflectarray containing this individual element [3]

After arranging the resonant elements as a multi-level Fresnel zone plate, the focusing is produced by the appropriate effect of the geometry of the Fresnel arrangement and the phase induced by the resonant elements [11], which can be characterized by a complex reflection coefficient. As far as the resonant elements behave differently as a function of the angle of incidence, polarization state, and wavelength, all these parameters will affect the image quality of the system. Once the complex reflection coefficient is obtained, the point spread function (PSF) is calculated using a Rayleigh–Sommerfeld propagation

algorithm to reach the focal region [12]. The modulation transfer function (MTF) is then evaluated from the PSF as a function of the $F/\#$, polarization, and wavelength [13].

In Section 2, we present a monochromatic analysis of the MTF as a function of the $F/\#$ and polarization. The polychromatic MTF is calculated in Section 3, assuming that the angle and the state of polarization do not affect the results, which assumption is most accurate for high $F/\#$ systems. The Strehl ratio is also used in the chromatic analysis of reflectarrays as an additional figure of merit of the image quality of the system. The main conclusions of this manuscript are then summarized in Section 4.

2. Image Quality for Monochromatic Illumination

As is well known [13], the properties of a linear imaging system are specified by the PSF, which is computed as the system response for an input impulse (Dirac delta function). For a mirror reflectarray imaging an object at the infinity, calculating PSF is equivalent to calculating the image when a monochromatic on-axis plane wave is entering the system, so it is necessary to propagate the electric field distribution from the system's exit pupil to the image plane. To do this, we have numerically solved the

Rayleigh–Sommerfeld diffraction equation using the procedure described by Shen and Wang [12]. Therefore, in this work we will rely on the scalar diffraction theory, although we will introduce some polarization information through the reflection properties of the reflect array.

For calculating the PSF, we will use the coordinate system depicted in Fig. 2, so the reflectarray is located at the $x_0 - y_0$ plane while the point object is placed on the z axis (we are considering only object points placed along the optical axis of the system). Let us define $E_0(x_0, y_0)$ as the electric field coming from the object point that is incident on the entrance pupil of the reflectarray. As we are considering the reflectarray as a flat mirrorlike object, we will characterize it by a complex reflection coefficient $\rho(x_0, y_0)$. Under these conditions, the reflected electric field at the reflectarray's exit pupil is $E_{r0}(x_0, y_0) = \rho(x_0, y_0)E_0(x_0, y_0)$. Thus, the reflected field E_r at the point with coordinates (x, y, z) is given by [12]

$$E_r(x, y, z) = \iint_A E_{r0}(x_0, y_0) \cdot \frac{\exp(jkr)}{2\pi \cdot r} \frac{z}{r} \times \left(\frac{1}{r} - jk \right) dx_0 dy_0, \quad (1)$$

where A is the aperture of the reflectarray and $r = \sqrt{(x - x_0)^2 + (y - y_0)^2 + z^2}$. The PSF can be calculated from the electric field as

$$\text{PSF}(x, y, z) = \|E_r(x, y, z)\|^2|_{O_p}, \quad (2)$$

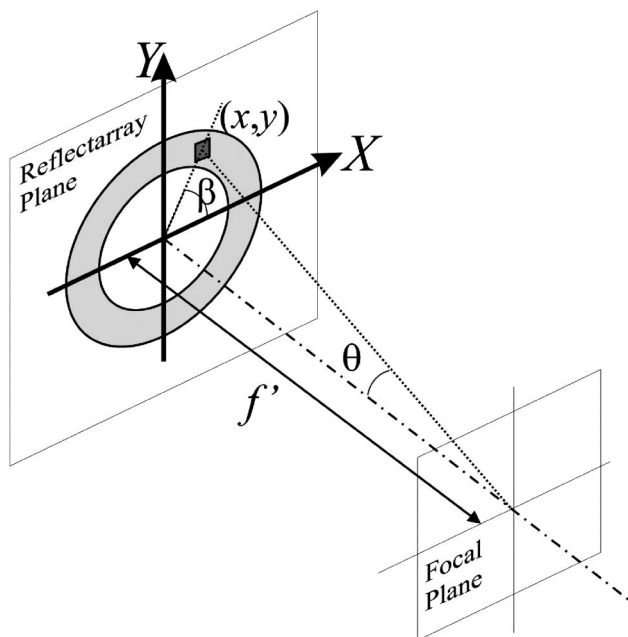


Fig. 2. Typical layout of a reflectarray focusing onto a plane. The resonant element is represented as the dark gray square on a circular ring at the reflectarray plane. The angle θ describes the location of a given point of the reflectarray with respect to the focal point of the system.

where O_p indicates a point object. The dependence of PSF on the z coordinate allows us to consider the effect of defocus on the reflectarray's image quality. It should be stressed that using Eq. (1) implies that we are dealing with a monochromatic input field so both the reflected field and PSF are functions of the wavelength, although it has not been explicitly stated in Eqs. (1) and (2).

A further modification of our method can be introduced in order to deal with vector properties such as light polarization, accounting for polarization effects through the complex reflection coefficient function $\rho(x_0, y_0)$ and the Jones vector formalism as described in [3]. Let us suppose that the vector incident field is given by a Jones vector:

$$\mathbf{E}_0(x_0, y_0) = \begin{bmatrix} E_{0x}(x_0, y_0) \\ E_{0y}(x_0, y_0) \end{bmatrix}. \quad (3)$$

On the other hand, we have characterized the reflectarray by a complex reflection coefficient function that is polarization dependent, so we have two components, $\rho_{\perp}(x_0, y_0)$ and $\rho_{\parallel}(x_0, y_0)$, for perpendicular and parallel polarization to the incident plane, respectively. These reflection coefficients have been calculated using HFSS and Designer packages as previously stated. We have to state that, for the case of off-axis incidence, the definition of the plane of incidence to describe the polarization states should be reconsidered in order to comply with the coplanarity condition for the incident and reflected ray vector and the normal vector to the reflectarray plane. Let us recall again that, although not explicitly stated, both incident field and complex reflection coefficient are wavelength dependent. With these assumptions, we calculate the reflected electric field at the reflectarray plane as

$$\begin{bmatrix} E_{r0x} \\ E_{r0y} \end{bmatrix} = \mathbf{R}^{-1}(\beta(x_0, y_0)) \cdot \begin{bmatrix} \rho_{\parallel}(x_0, y_0) & 0 \\ 0 & \rho_{\perp}(x_0, y_0) \end{bmatrix} \cdot \mathbf{R}(\beta(x_0, y_0)) \begin{bmatrix} E_{0x}(x_0, y_0) \\ E_{0y}(x_0, y_0) \end{bmatrix}, \quad (4)$$

where \mathbf{R} is the two-dimensional rotation matrix and $\beta(x_0, y_0)$ is the azimuth angle as seen in Fig. 2. Once we have calculated the components of the reflected electric field at the exit pupil of the reflectarray, we propagate each component independently using Eq. (1) and calculate the PSF. Afterwards, in order to estimate the image quality of the reflectarray, we compute the MTF as the modulus of the complex optical transfer function $H(\nu_x, \nu_y)$ obtained through the Fourier transform of the PSF [13]:

$$H(\nu_x, \nu_y) = \iint \text{PSF}(x, y, z) \exp(-i \cdot 2\pi \cdot (\nu_x x + \nu_y y)) dx dy. \quad (5)$$

Following the calculation procedure described in the preceding paragraphs, we have evaluated the image

quality at the focal plane ($z = f$) of a reflectarray as a function of the aperture, specified by an $F/\#$ ranging between 0.23 and 8.68. We have considered an incident collimated beam linearly polarized and we have studied two cases corresponding to horizontal and vertical polarization. Our reflectarray has been designed for a wavelength of $10.6 \mu\text{m}$ with a focal length (at the design wavelength) of 152.6 mm .

We have previously shown that the irradiance pattern at the focal point loses its radial symmetry due to the polarization effects [3]. In Fig. 3(a), we show the horizontal profile of the PSF obtained for both polarizations for the maximum aperture studied ($F/\# = 0.23$). A slight difference between the two profiles can be observed, with the horizontal profile being narrower than the vertical one. The corresponding horizontal profiles of the two MTFs are depicted in Fig. 3(b). From this plot, we can conclude that even for this low $F/\#$, the incident field polarization has little influence on image quality, although the resolution limit along the horizontal direction is slightly lower for the horizontal polarization.

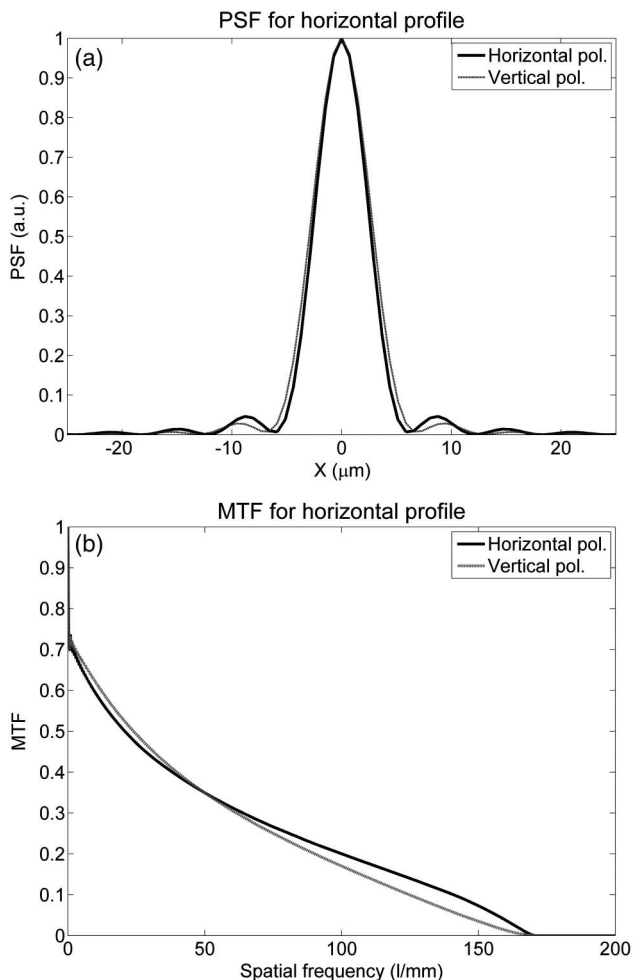


Fig. 3. (a) PSF and (b) MTF for a large aperture reflectarray as a function of the polarization state of the incident radiation. The cutoff frequency is the same for the two polarizations but the MTF behaves differently.

Another conclusion that can be drawn from the profiles of Fig. 3(b) is that the MTF obtained is worse than the one predicted for an ideal system at the diffraction limit. Therefore, there is a loss of image quality due to the aberrations introduced by the complex reflection coefficient function for this low $F/\#$.

For a higher $F/\#$, we obtain the plots in Fig. 4(a), where the reflectarray presents a better image quality because the MTF profiles are closer to the ideal system, but at the same time, the resolving power (given by the MTF cutoff frequency) decreases. The increment of image quality can be seen clearly in Fig. 4(b) where we show, as a function of $F/\#$, the ratio between the area of the horizontal MTF profile obtained for the reflectarray and the area of the MTF corresponding to a diffraction-limited system with the same aperture. We can see in Fig. 4(b) how the area quotient becomes closer to 1 as the $F/\#$ increases, indicating a net gain of image quality. This fact can be explained because with a higher $F/\#$, the effect of aberrations is reduced. On the other hand, diffraction effects become more noticeable, so the extent of the PSF is increased and, consequently, the

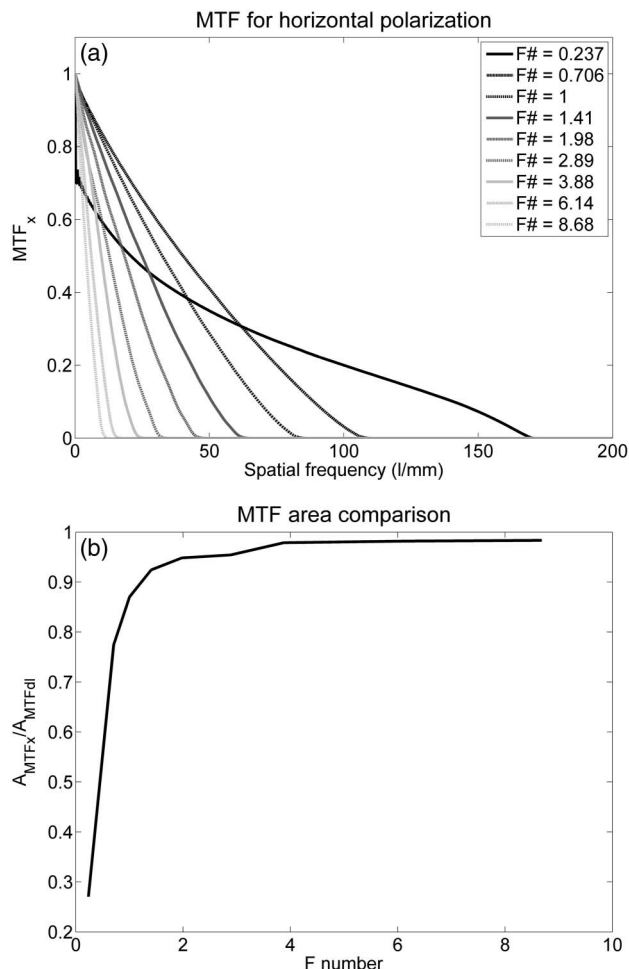


Fig. 4. (a) Horizontal profile of the MTF for horizontal linear polarization as a function of the $F/\#$. (b) Ratio between the area under the calculated MTF and the diffraction-limited MTF as a function of the $F/\#$.

MTF cutoff frequency (resolving power) drops. Therefore, attending to image quality criteria, the reflectarray behaves in the same way as other image formation systems.

As a practical consequence, a compromise must be made between the aperture size of the reflectarray in order to get the maximum image quality with the greatest aperture possible. In this way, Fig. 4(b) could be of use to determine such a compromise. In our example, it can be observed that for $F/\#$ higher than 4, there is no gain in image quality, so the optimum $F/\#$ value (regardless of other considerations such as illumination, etc.) should not be higher than 4 in order to meet the best compromise between image quality and aperture.

3. Polychromatic Image Quality

The analysis of the polychromatic behavior of the reflectarray is made using the same formalism as in the case of a monochromatic input. An input monochromatic plane wave impinges on the reflectarray and the given image is obtained. However, as the diffractive design is strongly dependent on wavelength, the image is obtained for a collection of planes along the propagation axis and not just at the designed focal length. On the other hand, the reflectarray is typically designed to perform the best at a specified wavelength, for which a nominal focal length is defined. The chromatic properties of the Fresnel layout can then be expressed as the following dependence:

$$f(\lambda) = \frac{f_d \lambda_d}{\lambda}, \quad (6)$$

where f_d is the nominal focal distance for a design wavelength λ_d . Figure 5(a) shows the irradiance as a function of the wavelength and the axial coordinate. The maximum is located at those points given by Eq. (6). On the other hand, the value of the maximum of irradiance as a function of λ , plotted in Fig. 5(b), has a dependence that follows the chromatic behavior of the modulus of the reflection coefficient of the resonant elements [see Fig. 1(c)].

A. Strehl Ratio for Reflectarrays

To begin the analysis of the image quality as a function of the wavelength, we first calculate the Strehl ratio [14] and provide a wavelength range where the Strehl ratio is higher than a predefined value.

The chromatic change in intensity at the focal point is approximately given as a Taylor expansion around the wavelength where the maximum is reached as

$$I(\lambda) = I_d + \frac{\partial I}{\partial \lambda} \Big|_{\lambda=\lambda_{\max}} \Delta\lambda + \frac{1}{2} \frac{\partial^2 I}{\partial \lambda^2} \Big|_{\lambda=\lambda_{\max}} (\Delta\lambda)^2. \quad (7)$$

The Strehl ratio is then defined as $S = \frac{I(\lambda)}{I_d}$. Because the situation at $\lambda = \lambda_{\max}$ is that of a maximum of irradiance, then analytically we may assume that the first derivative is zero and the second derivative

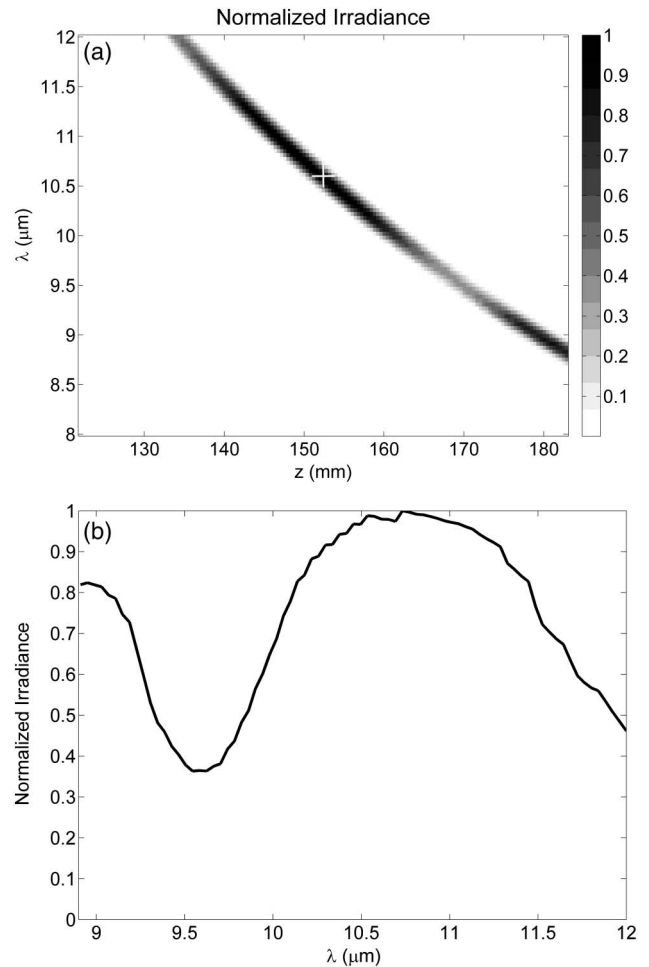


Fig. 5. (a) Irradiance map as a function of the axial coordinate z and λ . The white cross represents the point corresponding to the design conditions. (b) Plot of the evolution of the irradiance at the location given by Eq. (3).

is negative. Therefore, the Strehl ratio is given as a quadratic function in $\Delta\lambda = \lambda - \lambda_{\max}$:

$$S = 1 + \frac{1}{2I_d} \frac{\partial^2 I}{\partial \lambda^2} \Big|_{\lambda=\lambda_{\max}} (\Delta\lambda)^2. \quad (8)$$

From the numerical results obtained for the fabricated reflectarray, having an $F/6$ aperture, we may evaluate this second derivative. After this calculation, we found that the Strehl ratio falls to 0.8 when $\Delta\lambda = 79.2$ nm, showing the strong chromatic dependence of the system. This corresponds with a 0.7% relative change in wavelength. This result is slightly different for each wavelength.

B. Polychromatic MTF

After obtaining the spectral complex reflection coefficient map, $\rho(x, y, \lambda)$, we simulate the focusing properties of this reflectarray for a collimated incident beam of uniform irradiance aligned with the optical axis and having an aperture of $F/6$. We propagate this field to a focus plane located at a distance z from the reflectarray using a Rayleigh–Sommerfeld

algorithm [12]. Figure 5(a) shows the distribution of the on-axis irradiance on the image plane as a function of the axial coordinate z (longitudinal chromatic aberration) and wavelength λ . The plot shows that, because of the dispersive nature of the resonant elements seen in Fig. 1, the on-axis irradiance is not the same for each wavelength. The decrease in focused irradiance observed around $\lambda = 9.5 \mu\text{m}$ can be explained by the decrease in the magnitude of the complex reflection coefficient. We have verified by calculation that even though the relative shifts between successive zones may strongly depart from the nominal case [as shown in Fig. 1(d)], the focusing is mainly driven by the Fresnel subzone arrangement and by the magnitude of the reflection coefficients. This is shown in Fig. 5(b). Only when the interzone phase increment significantly departs from the nominal one (45°) does the maximum irradiance decrease. Figure 5(a) also shows that, for a fixed image plane, the image quality will change rapidly when the wavelength changes. To illustrate this, we plot in Fig. 6(a) the MTF at the focal plane for several wavelengths around λ_d . The MTF for $\lambda_d = 10.6 \mu\text{m}$

is nearly that of a perfect system that corresponds to the almost diffraction-limited PSF for an $F/6$ system, as shown in Fig. 4(b). However, when the wavelength departs from the design wavelength, the reflectarray shows significant chromatic aberration. The chromatic aberration can be interpreted as a wavelength-dependent defocus (axial chromatic aberration). Therefore, for a different location of the image plane, the best image quality will be obtained for a wavelength different from λ_d . In Fig. 6(b), we plot the MTF for a given frequency (one-third of the cutoff frequency obtained at λ_d) for different wavelengths at two different locations, the focal plane $z_1 = f_d = 0.1524 \text{ m}$ and a plane placed at a distance $z_2 = 0.1753 \text{ m}$ from the reflectarray. The result shows that, for the focal plane, the maximum MTF is obtained for λ_d , while for the second plane, the wavelength that gives the maximum MTF is $\lambda = 9.2 \mu\text{m}$, as predicted by Eq. (6). The dispersion of the sub-wavelength elements makes these two profiles different.

4. Conclusions

The resonant elements that constitute an infrared reflectarray have functional dependence on angle, polarization state, and wavelength. The effect of this dependence on the quality of the images given by reflectarrays has been analyzed for a focusing reflectarray in the infrared. The MTF has been calculated from a PSF evaluated using a Rayleigh–Sommerfeld approach, adapted to deal with polarization within a Jones formalism.

For monochromatic illumination, we verified that the MTF is quite similar to the diffraction-limited one. When comparing the actual and diffraction-limited MTFs for the same $F/\#$ we found that for $F/\#$ greater than 2, the ratio between the area under the MTF is larger than 0.95, maintaining a high and constant value when $F/\# \geq 4$. When considering polarization only for very low $F/\#$ (large apertures), we find a nonnegligible difference between the horizontal and vertical polarizations in the MTF. At the same time, those MTFs for very low $F/\#$ are well below the diffraction-limited MTF even for low frequency components. The chromatic dependence of reflectarrays is strongly affected by the Fresnel zone arrangement of the resonant elements. The calculation of the Strehl ratio shows that it decays to 0.8 when the wavelength has 0.7% of relative change. This value indicates a strong chromatic dependence. This can be also seen when evaluating the MTF at several wavelengths. The almost diffraction-limited behavior is significantly degraded when the wavelength changes around the design wavelength. The chromatic change can be only compensated when moving the plane of interest to the location predicted by the diffraction theory. The behavior at the best focus plane follows a dependence that resembles the chromatic change in the modulus of the reflection coefficient of the resonant structures.

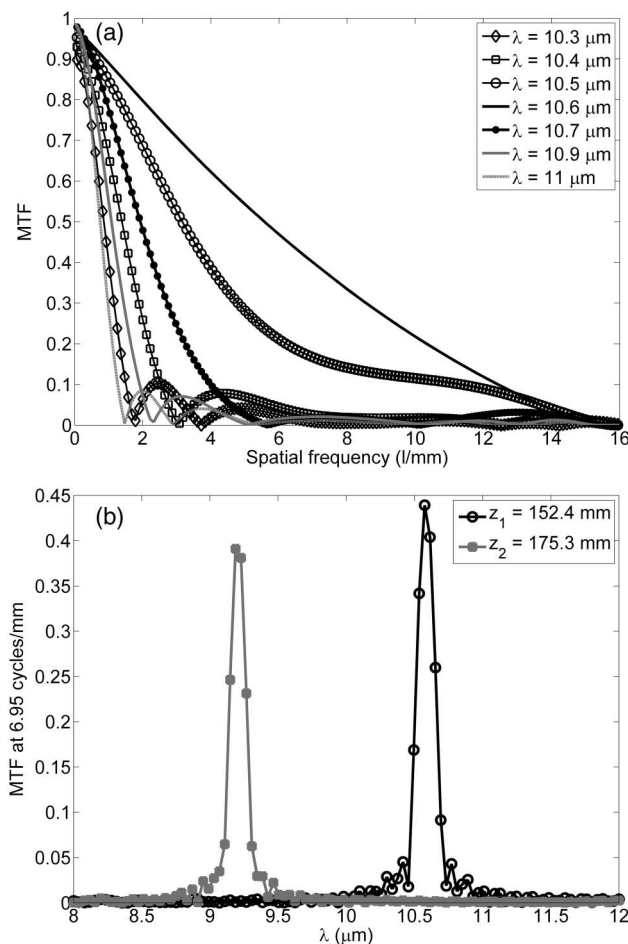


Fig. 6. (a) MTF for different wavelengths at the location of the nominal focus. MTF for a multilevel reflectarray at the focal planes for different wavelengths. (b) Chromatic dependence of the MTF at 6.95 cycles/mm for two axial positions.

Summarizing, we may conclude that the image quality of multilevel reflectarrays almost reaches the diffraction-limited behavior for medium and small apertures ($F/\# > 4$). The angular and polarization dependence is only significant for large aperture elements. On the other hand, due to the Fresnel zone arrangement of the resonant elements, the chromatic behavior is quite strong.

This work has been partially supported by the Spanish Ministry of Science under the project ENE2009-14340.

References

1. J. Ginn, B. Lail, and G. Boreman, "Phase characterization of reflectarray elements at infrared," *IEEE Trans. Antennas Propag.* **55**, 2989–2993 (2007).
2. J. Ginn, B. Lail, J. Alda, and G. Boreman, "Planar infrared binary phase reflectarray," *Opt. Lett.* **33**, 779–781 (2008).
3. J. Ginn, J. Alda, J. A. Gómez-Pedrero, and G. Boreman, "Monochromatic aberrations in resonant optical elements applied to a focusing multilevel reflectarray," *Opt. Express* **18**, 10931–10940 (2010).
4. B. Munk, *Finite Antenna Arrays and FSS* (Wiley, 2006).
5. J. Tharp, J. M. Lopez-Alonso, J. Ginn, C. Middleton, B. Lail, B. Munk, and G. Boreman, "Demonstration of a single-layer meanderline phase retarder at infrared," *Opt. Lett.* **31**, 2687–2689 (2006).
6. J. Tharp, J. Alda, and G. Boreman, "Off-axis behavior of an infrared meanderline waveplate," *Opt. Lett.* **32**, 2852–2854 (2007).
7. D. Berry, R. Malech, and W. Kennedy, "The reflectarray antenna," *IEEE Trans. Antennas Propag.* **11**, 645–651 (1963).
8. D. Pozar and T. Metzler, "Analysis of a reflectarray antenna using microstrip patches of variable size," *Electron. Lett.* **29**, 657–658 (1993).
9. J. Huang and J. A. Encinar, *Reflectarray Antennas* (Wiley-IEEE, 2007).
10. F. J. González, J. Alda, J. S. Rodríguez, J. Ginn, and G. Boreman, "The effect of metal dispersion on the resonance of antennas at infrared frequencies," *Infrared Phys. Technol.* **52**, 48–51 (2009).
11. H. Hristov, *Fresnel Zones in Wireless Links, Zone Plates Lenses and Antennas* (Artech, 2000).
12. F. Shen and A. Wang, "Fast-Fourier-transform based numerical integration method for the Rayleigh–Sommerfeld diffraction formula," *Appl. Opt.* **45**, 1102–1110 (2006).
13. J. W. Goodman *Introduction to Fourier Optics*, 3rd ed. (Roberts, 2005).
14. V. N. Mahajan, "Strehl ratio for primary aberrations: some analytical results for circular and annular pupils," *J. Opt. Soc. Am.* **72**, 1258–1266 (1982).